Miao Liu,[1] Nirmal Verma,[1] Xiaoli Peng,[1] Sarah Srodulski,[1] Andrew Morris,[2] Martin Chow,[3] Louis B. Hersh,[3] Jing Chen,[3] Haining Zhu,[3] Mihai G. Netea,[4] Kenneth B. Margulies,[5] Sanda Despa,[1] and Florin Despa[1]

Hyperamylinemia Increases IL-1β Synthesis in the Heart via Peroxidative Sarcolemmal Injury

Diabetes 2016;65:2772–2783 | DOI: 10.2337/db16-0044

COMPLICATIONS

Hypersecretion of amylin is common in individuals with prediabetes, causes amylin deposition and proteotoxicity in pancreatic islets, and contributes to the development of type 2 diabetes. Recent studies also identified amylin deposits in failing hearts from patients with obesity or type 2 diabetes and demonstrated that hyperamylinemia accelerates the development of heart dysfunction in rats expressing human amylin in pancreatic β-cells (HIP rats). To further determine the impact of hyperamylinemia on cardiac myocytes, we investigated human myocardium, compared diabetic HIP rats with diabetic rats expressing endogenous (nonamyloidogenic) rat amylin, studied normal mice injected with aggregated human amylin, and developed in vitro cell models. We found that amylin deposition negatively affects cardiac myocytes by inducing sarcolemmal injury, generating reactive aldehydes, forming amylin-based adducts with reactive aldehydes, and increasing synthesis of the proinflammatory cytokine interleukin-1β (IL-1β) independently of hyperglycemia. These results are consistent with the pathological role of amylin deposition in the pancreas, uncover a novel contributing mechanism to cardiac myocyte injury in type 2 diabetes, and suggest a potentially treatable link of type 2 diabetes with diabetic heart disease. Although further studies are necessary, these data also suggest that IL-1β might function as a sensor of myocyte amylin uptake and a potential mediator of myocyte injury.

Amylin (also known as islet amyloid polypeptide) is a regulatory peptide synthesized and cosecreted with insulin by pancreatic β-cells and is believed to participate in promoting satiety by slowing gastric emptying (1). Like insulin, amylin is oversecreted in patients with obesity or prediabetic insulin resistance (i.e., hyperinsulinemia coincides always with hyperamylinemia). Elevated human amylin secretion promotes its deposition in the pancreas (1), which induces oxidative stress (2), activation of the NLRP3 inflammasome, and release of interleukin (IL)-1β (3), a cytokine involved in a plethora of inflammatory responses (4). Thus, hyperamylinemia is a critical early contributor to the development of type 2 diabetes. The pathological effects of hyperamylinemia were thought to be limited to pancreatic islets. However, recent studies (5–10) found amylin deposition in failing kidneys (5) and hearts (6,7) from patients with type 2 diabetes, and in the brains (8–10) of patients with diabetes who have Alzheimer's disease. In the heart, significant amylin deposits were identified in areas of cardiac myocyte injury (6,7) and in myocyte lysates (7), suggesting a role in the pathogenesis of diabetic heart disease. Amylin deposition in the pancreas and in extrapancreatic tissues, including the heart, was mirrored in a rat model of type 2 diabetes expressing human amylin in the pancreas (HIP) (6,7,11–16). HIP rats develop type 2 diabetes (14) cardiovascular dysfunction (6,7,12–14), neuroinflammation (11,15), and neurologic deficits (11). Particularly, the HIP rats show diastolic dysfunction (6), cardiac hypertrophy (7), and cardiac dilation (7), which resemble some of the pathogenic mechanisms of diabetic cardiomyopathy in humans (17). Thus, hyperamylinemia contributes to pathogenic pathways for both type 2 diabetes and the co-occurring

[1]Department of Pharmacology and Nutritional Sciences, College of Medicine, University of Kentucky, Lexington, KY
[2]Division of Cardiovascular Medicine, Gill Heart Institute, University of Kentucky, Lexington, KY
[3]Department of Molecular and Cellular Biochemistry, College of Medicine, University of Kentucky, Lexington, KY
[4]Department of Internal Medicine, Radboud University Nijmegen Medical Center, Nijmegen, the Netherlands
[5]Cardiovascular Research Institute, Perelman School of Medicine, University of Pennsylvania, Philadelphia, PA

Corresponding author: Florin Despa, f.despa@uky.edu.

Received 9 January 2016 and accepted 9 June 2016.

This article contains Supplementary Data online at http://diabetes.diabetesjournals.org/lookup/suppl/doi:10.2337/db16-0044/-/DC1.

cardiac disease. Similar intertissue communication was previously (18) shown to connect Alzheimer's disease with skeletal muscle disorders in aged humans.

The toxicity of amylin from humans (and a few other species) (1) was linked to amyloidogenicity (1) and an increased propensity to aggregate and interact with cellular membranes (19–21). Aggregated amylin disrupts membrane integrity, ion homeostasis, and cell function (1,19–21). The role of amyloidogenicity in amylin-induced toxicity is supported by the observation (21) that, in contrast to HIP rats, rodents overexpressing rodent amylin, which is not amyloidogenic (1), showed neither amylin deposition nor development of type 2 diabetes.

Disrupting membrane integrity by the incorporation of aggregated amylin could also increase the exposure of unsaturated fatty acids to cytosolic reactive oxygen species (ROS). This process leads to the formation of reactive aldehydes (22), such as 4-hydroxy-2-nonenal (4-HNE) and malondialdehyde (MDA). Although the generation of reactive aldehydes is essential for cell survival signaling (22), increased levels of 4-HNE and MDA further elevate ROS and trigger inflammatory responses (22). 4-HNE and MDA can also nonenzymatically form stable protein adducts by binding to histidine, lysine, and cysteine side chains (i.e., the Maillard reaction) (22). 4-HNE– and MDA-modified proteins have been used as biomarkers for cell oxidative damage (22). We therefore hypothesize that myocardial amylin deposition destabilizes the sarcolemma and generates reactive aldehydes that perturb intracellular homeostasis, leading to increased synthesis of IL-1β. To test this hypothesis, we analyzed tissue specimens from humans, compared human amylin–expressing (HIP) rats with age- and glucose-matched diabetic rats expressing only endogenous nonamyloidogenic rat amylin, studied mice injected with aggregated human amylin, and developed in vitro cell models.

RESEARCH DESIGN AND METHODS

The investigation conforms to the *Guide for the Care and Use of Laboratory Animals* published by the U.S. National Institutes of Health (NIH Publication No. 85–23, revised 1996) and was approved by the Institutional Animal Care and Use Committees at the University of Kentucky.

The protocol concerning the use of biopsy samples from patients was approved by the Institutional Review Board at the Hospital of the University of Pennsylvania, and informed consent was obtained prospectively in all cases.

Human Samples

Human specimens used in this study were also used in the cohorts reported in our previous publications (6,7). Myocardial samples were obtained from obese individuals (BMI $\geq$30 kg/m^2) with nonischemic heart failure (O-HF) (n = 7) and patients with type 2 diabetes and nonischemic heart failure (D-HF) (n = 5). Overt type 2 diabetes developed during the early post-transplantation period in patients in the O-HF group. Hence, we speculated that these patients were in prediabetes at the time of heart transplantation. Nonfailing hearts from lean donors without diabetes formed the control (Ctl) group (n = 7).

Experimental Animals

Rats that express human amylin in the pancreatic β-cells (HIP rats, n = 25; Charles River Laboratories) were used as type 2 diabetic animals with myocardial amylin deposition (6,7). They were generated from Sprague Dawley rats by expressing human amylin on the insulin promoter (16). HIP rats used in this study were ~10 months of age and displayed nonfasting blood glucose levels (morning time) in the 300–400 mg/dL concentration range. Age-matched wild-type (WT) (n = 30) littermates were used as nondiabetic Ctl animals. Ideal diabetic Ctl rats for this study should have a Sprague Dawley genetic background and develop type 2 diabetes spontaneously (with a regular diet) on the same timeline as HIP rats. However, such a model is not feasible because rats do not develop type 2 diabetes spontaneously (1). We therefore used UCD rats (n = 12), which have half of Sprague Dawley genes and develop type 2 diabetes (7,23). The other half of their genes are from the Zucker diabetic-lean rat, a rat model that displays a proinsulin defect in pancreatic β-cells and intact leptin receptor function (24). Changes in blood insulin and amylin levels in HIP and UCD rats with the transition from normal to prediabetes and full-blown diabetes were published elsewhere (7,11,23).

C57BL/6 mice were intravenously injected (via tail vein) with either aggregated human amylin (2 μg/g body wt; n = 8) or saline (n = 8) for 5 days (twice a day) followed by 14 days of intraperitoneal injections.

Proteomics

Amylin-positive protein fractions from myocardial lysates were isolated using high-performance liquid chromatography (HPLC) and further analyzed by liquid chromatography–tandem mass spectrometry (LC-MS/MS). A Waters 717 plus HPLC system (5 μm; 4.6 mm × 5 cm; C18 column; Phenomenex) with a 15-min linear gradient from 5% to 75% mobile phase B (0.1% trifluoroacetic acid in acetonitrile) was used for separation of amylin-positive fractions. The mobile phase A was 0.1% (v/v) trifluoroacetic acid in water, and the flow rate was set at 1 mL/min. Amylin was detected with a diode array detector at 214 nm, and fractions were collected. Amylin-containing tissue fractions were confirmed by comparison with an amylin standard.

For the LC-MS/MS test, we used an LTQ-Orbitrap Mass Spectrometer (ThermoFisher Scientific, Waltham, MA) coupled with a Nanoflex cHiPLC System (Eksigent Technologies, Dublin, CA) through a nanoelectrospray ionization source (25). Data were acquired in an automated data-dependent acquisition mode consisting of an Orbitrap MS scan (300−1,800 charge/mass ratio [m/z], 60,000 resolutions) followed by MS/MS for fragmentation of the 7 most abundant ions with the collision induced dissociation method. The 4+ ion of amylin peptide (m/z = 976.22) was extracted from the total ion spectrum. The MS/MS fragments of amylin were confirmed by comparison with an amylin standard.

Metabolomics

Heart homogenates were derivatized with 2,4-dinitrophenylhydrazine (DNPH) (for MDA analysis), extracted with ethyl acetate, dried under nitrogen, and reconstituted with acetonitrile (26). Analysis of MDA-DNPH and 4-HNE-reduced glutathione (GSH) was carried out using a Shimadzu ultrafast liquid chromatography system coupled with an AB Sciex 4000-Qtrap hybrid linear ion trap triple-quadrupole mass spectrometer in multiple reaction–monitoring mode. MDA-DNPH and GSH-HNE were analyzed using a Machery-Nagel Nucleodur C8 Gravity column (5 μm, 125 × 2.0 mm).

Immunochemistry

Thin sections of paraffin-embedded tissues were incubated with a combination of anti–human amylin (SC-377530; Santa Cruz Biotechnology, Dallas, TX) and anti–4-HNE (ab46545; Abcam, Cambridge, U.K.), anti-MDA (ab94671; Abcam), or anti–IL-1β (ab9722; Abcam) primary antibodies. After washings, sections were incubated with Alexa Fluor 488–conjugated anti-mouse IgG (A11029; Invitrogen, Carlsbad, CA) and Texas Red–conjugated anti-rabbit IgG (SC-2780; Santa Cruz Biotechnology) secondary antibodies. The sections were then stained with DAPI (ab104139; Abcam) and imaged with a laser-scanning confocal microscope (Live5; Zeiss, Oberkochen, Germany). Elastin autofluorescence was blocked with 1% Sudan Black. Immunofluorescence measurements were also performed on fixed myocytes incubated with anti–IL-1β primary antibodies and Alexa Fluor 488–conjugated secondary antibodies. Western blot analysis was performed on tissue homogenates and lysates from cardiac myocytes. After electrophoresis, blotting, and blocking, membranes were incubated with primary antibodies for amylin (T-4157; Bachem, Bubendorf, Switzerland), 4-HNE, MDA, IL-1β (all three obtained as cited above), tumor necrosis factor-α (TNF-α) (ab1793; Abcam), IL-6 (ab9324; Abcam), IL-10 (ab25073; Abcam), or GAPDH (ab8245; Abcam [loading Ctl for heart samples]). The specific staining of protein bands was verified as previously described (6–8). The total amylin level in plasma was assessed by ELISA (EZHAT-51K; EMD Millipore, Billerica, MA).

In some experiments, 4-HNE or MDA were immunoprecipitated using the same antibodies as above and immobilized protein A/G resin slurry (catalog #20421; ThermoFisher Scientific).

Quantitative real-time PCR (RT-PCR) was used to assess the mRNA level of IL-1β in myocardial tissues as previously described (8).

Cell isolation was performed as previously described (6,7,27).

Measurement of Lipid Peroxidation in Isolated Cells

Isolated myocytes were incubated for 2 h under Ctl conditions, with aggregated amylin and/or 400 mg/dL glucose, with 50 μmol/L poloxamer 188 for 2 h followed by aggregated amylin, and with 5 mmol/L *N*-acetyl cysteine (NAC) for 30 min followed by aggregated amylin. After incubation, myocytes were loaded with the fluorescent probe 4,4-difluoro-5-(4-phenyl-1,3-butadienyl)-4-bora-3a,4a-diaza-s-indacene-3-undecanoic acid (C_{11}-BODIPY$^{581/591}$; catalog #D3861; Invitrogen) and imaged with a confocal microscope (Live5; Zeiss). Upon peroxidation, the fluorescence emission peak of C_{11}-BODIPY$^{581/591}$ shifts from 590 nm (red) to 510 nm (green). Thus, lipid peroxidation was measured as the ratio between the average fluorescence intensity in the green and red channels.

Proximity Ligation Assay

For the Duolink in situ proximity ligation assay (PLA), sections were incubated for 90 min with oligonucleotide-conjugated anti-mouse IgG MINUS (DUO92004; Sigma-Aldrich, St. Louis, MO) and anti-rabbit IgG PLUS (PLA probes; catalog #DUO92002, Sigma-Aldrich) diluted 1:6 in Tris-buffered saline at 37°C. Amplified DNA strands were detected with oligonucleotides conjugated to a fluorophore (Duolink In Situ Detection Reagents Red; catalog #DUO92008; Sigma-Aldrich). They were coverslipped with mounting medium DAPI (catalog #DUO82040; Sigma-Aldrich) and analyzed by confocal microscopy.

Langendorff Perfusion

To assess the dynamics of cardiac amylin deposition, isolated mouse hearts (n = 4) were perfused on a Langendorff apparatus with 10 μmol/L biotinylated human amylin in Tyrode solution for 2 h followed by a 10-min washout with Tyrode solution. Experiments were repeated with 10 μmol/L of aggregated amylin versus saline.

ROS production was measured as previously described (7).

Treatment

Poloxamer 188 is a surfactant that stabilizes lipid bilayers through hydrophobic interactions (28) and was used to block amylin-induced sarcolemmal damage in isolated cardiac myocytes (50 μmol/L; 2 h prior application of amylin). NAC was used to quench basal ROS production in Ctl myocytes (5 mmol/L; 30-min prior application of amylin).

Statistical Analysis

Data are presented as the mean ± SE. Statistical differences between groups were determined using *1*) an unpaired two-tailed Student t test when comparing two groups and *2*) a one-way ANOVA with Bonferroni post hoc test when comparing multiple groups, and were considered significant when $P < 0.05$.

RESULTS

Amylin Deposition in Human Hearts

Amylin and insulin have similar diurnal variation (29,30) and are elevated in individuals with obesity or prediabetic insulin resistance (31,32). Compared with Ctl subects, patients in the O-HF group showed elevated blood levels of amylin and insulin (Fig. 1*A*). Western blot analysis of blood, heart, and pancreas lysates identified multiple amylin aggregates and only a faint 4-kDa band corresponding to the monomeric amylin (Fig. 1*B*). Furthermore, aggregated amylin with similar molecular weights are seen in both blood and cardiac myocyte lysates. These results are consistent with our previous data from HIP rats (7) and

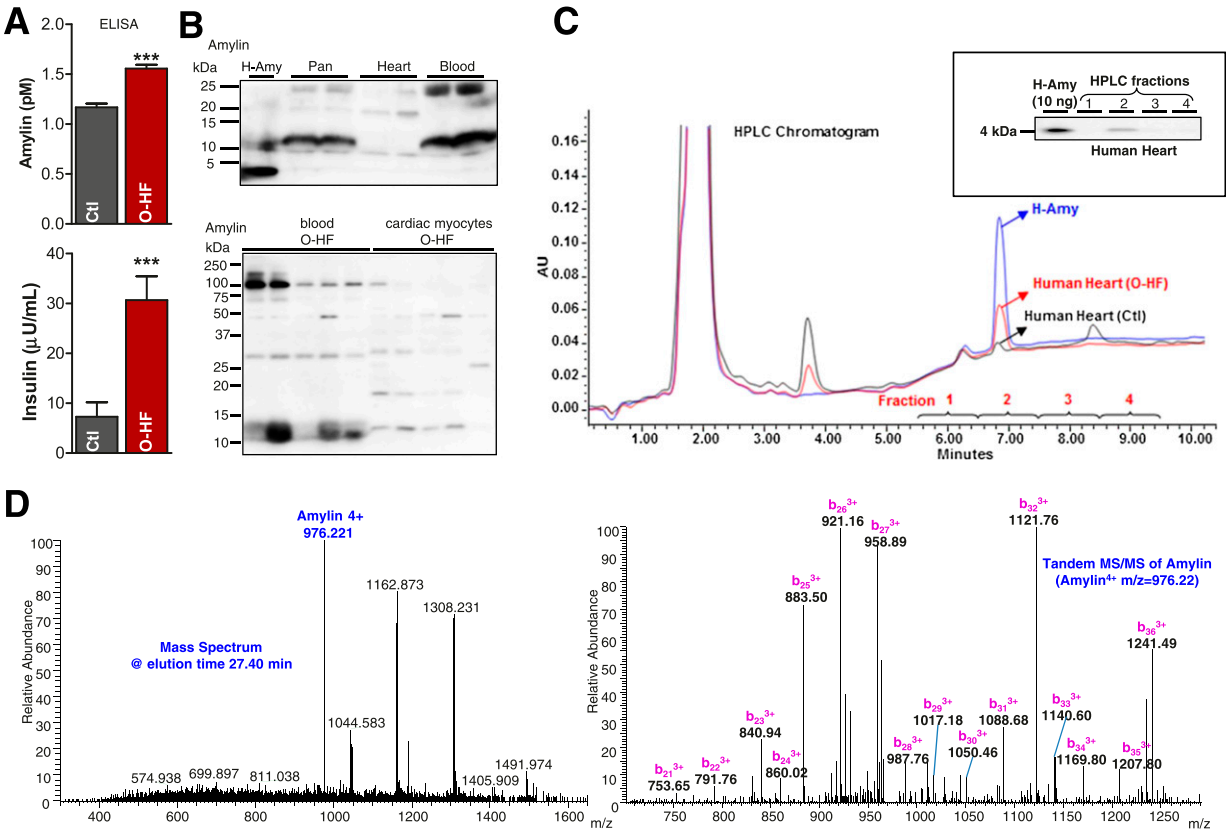

Figure 1—Testing the amylin deposition in human hearts. *A*: Blood amylin and insulin levels in patients with O-HF and Ctl subjects without diabetes were measured by ELISA (n = 7 samples/group). *B*: Top panel shows Western blot analysis of amylin in pancreas (Pan), blood, and cardiac tissue from humans. Freshly solubilized recombinant human amylin (H-Amy; 50 ng) and pancreatic tissue from a patient with type 2 diabetes were positive Ctls for monomeric amylin and aggregated amylin, respectively. In the bottom panel, we compared aggregated amylin in blood and cardiac myocytes from the O-HF group by Western blot. *C*: Typical reverse-phase HPLC chromatogram of human amylin standard human cardiac tissue. In the inset, selected fractions according to the retention time of human amylin standard were tested for the presence of amylin by Western blot. Ten nanograms of recombinant H-Amy was loaded as a positive Ctl. A representative blot from three independent experiments is shown. *D*: Fractions collected from HPLC (the amylin-positive fractions) were analyzed by LC-MS/MS. The representative mass spectrum of peptides eluted at 27.40 min shows the 4+ ion of amylin (m/z = 976.22). The right panel is the corresponding MS/MS spectrum of amylin. The fragments corresponding to the b ions are labeled, clearly proving that this peptide is amylin. AU, arbitrary units.

suggest that circulating aggregated amylin may promote myocardial amylin deposition. (Additional data are provided in the Supplementary Fig. 1.)

Next, we used proteomics to test the presence of amylin deposition in the heart. Based on the retention time of the standard amylin peptide, as derived from the HPLC chromatogram (Fig. 1*C*), we initially collected four different cardiac lysate fractions. These fractions were immunoblotted to identify the amylin (Fig. 1*C*, inset). The lysate fraction positive for amylin by Western blot also showed the presence of amylin by LC-MS/MS (Fig. 1*D*).

4-HNE-Amylin Adducts and Elevated Synthesis of IL-1β in Hearts of Patients With Diabetes

To test the formation of amylin-4-HNE and amylin-MDA adducts, we immunoprecipitated 4-HNE and MDA from cardiac myocyte lysates and used an ELISA to measure the amylin content in 4-HNE/MDA–enriched fractions. Amylin-4-HNE and amylin-MDA complexes were significantly elevated in hearts from the O-HF group (Fig. 2*A*). Thus, the incorporation of aggregated amylin in cardiac myocytes is associated with elevated levels of markers of peroxidative membrane injury. Furthermore, immunoconfocal microscopy analysis demonstrated that areas of myocyte amylin deposition were positive for both 4-HNE and MDA (Fig. 2*B*). In contrast, amylin-4HNE and amylin-MDA adducts were undetectable in myocardial tissue from the Ctl group. Pancreatic tissue from a patient with diabetes (positive Ctl for amylin deposition) also showed amylin-4-HNE/MDA colocalization (Fig. 2*C*).

Although cardiac myocytes are not major contributors to myocardial inflammation, they participate in the establishment of a proinflammatory environment under stress conditions by releasing cytokines and chemokines (33). IL-1β is part of the signaling pathway within myocytes that controls communication with leukocytes (33). The density of myocytes showing both amylin and IL-1β immunoreactivities was significantly higher in O-HF hearts compared with Ctl subjects (Fig. 2*D*), suggesting that myocyte

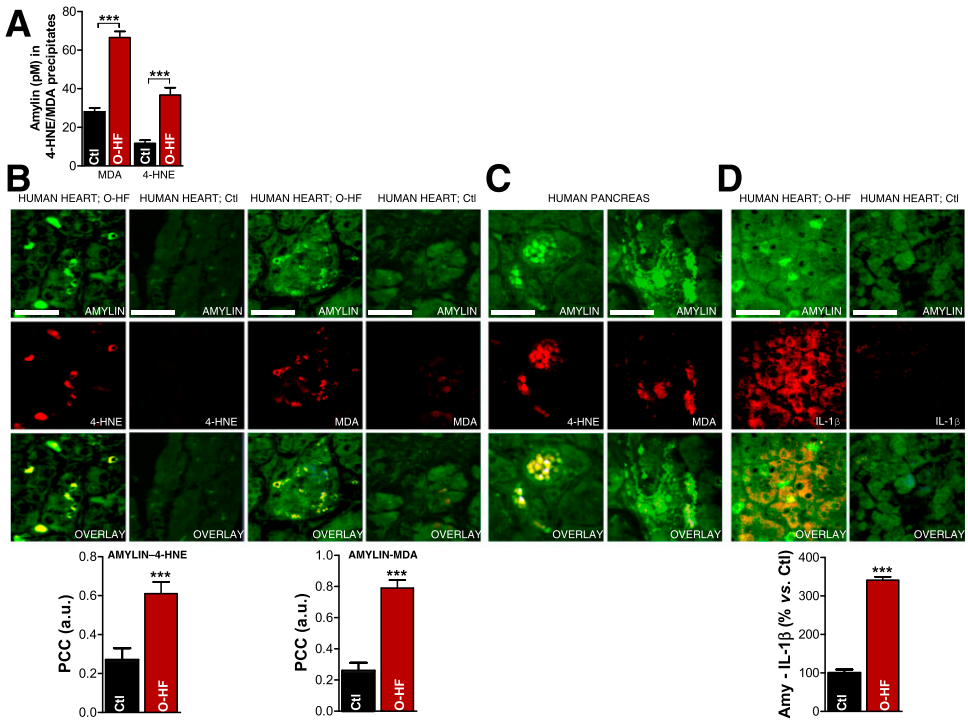

Figure 2— Failing hearts from obese patients display amylin-4-HNE and amylin-MDA adducts and increased IL-1β synthesis. *A*: 4-HNE and MDA were immunoprecipitated from heart homogenates. The level of amylin in the fractions enriched in 4-HNE and MDA was then quantified by ELISA. Dual-immunofluorescence staining of amylin (green) and 4-HNE or MDA (red) in the heart (*B*) and pancreas (*C*) of patients with O-HF (*B*), patients with type 2 diabetes (*C*), and Ctl subjects without diabetes (Ctl; *B*). Bar graphs in *B* display the mean pixel-by-pixel covariance in amylin and 4-HNE or MDA staining (Pearson's correlation coefficient [PCC]) in hearts from patients with O-HF vs. Ctl subjects. Scale bars, 20 μm. Ten sections per sample from $n = 4$ individuals in each group were investigated. *D*: Immunofluorescence staining of amylin (green) and IL-1β (red) in the heart specimens from O-HF patients and Ctl subjects. Bar graphs show the number of myocytes that are positive for both amylin and IL-1β in a 134 × 134 μm area in heart sections from patients with O-HF vs. Ctl subjects. Scale bars, 20 μm. Ten sections per sample from $n = 4$ individuals in each group were investigated. Data are presented as the mean ± SE. ***$P < 0.001$. a.u., arbitrary units.

uptake of amylin could trigger stress responses leading to exacerbated IL-1β synthesis, similar to amylin-mediated pathology in the pancreas (3).

We previously showed that failing hearts from patients with obesity or type 2 diabetes contain comparable levels of aggregated amylin (6). Amylin in myocardial fractions enriched in 4-HNE and MDA, the formation of amylin-4-HNE and amylin-MDA adducts, and IL-1β synthesis are all higher in the D-HF group compared with Ctl subjects (Fig. 3). This result suggests that obese individuals in whom type 2 diabetes developed shortly after heart transplantation and patients with pre-existing type 2 diabetes present similar relationships between amylin deposition and levels of reactive aldehydes and IL-1β.

4-HNE-Amylin Adducts in Hearts of Human Amylin–Expressing Diabetic Rats

HIP rat hearts show higher levels of 4-HNE and MDA compared with WT littermate rats (Fig. 4*A*). In contrast, cardiac 4-HNE and MDA in age- and glucose-matched UCD rats were comparable to those in the WT rats, indicating that, in the absence of amylin deposition, hyperglycemia does not cause significant lipid peroxidation in the heart. Using the same antibodies as cited above, we identified amylin-4-HNE adducts in HIP rat hearts, but not UCD rat hearts (Fig. 4*B*). The PLA signal shows an overall consistency with 4-HNE-amylin appearing in clusters in HIP rat hearts, which is consistent with the formation of adducts (Fig. 4*C*). Furthermore, Western blot analysis of heart lysates that were enriched in 4-HNE (and MDA) by immunoprecipitation demonstrated that amylin deposits in HIP rats underwent modifications by 4-HNE and MDA (Fig. 4*D*). Specifically, amylin-4-HNE and amylin-MDA complexes remained insoluble to sodium dodecyl sulfate and dithiothreitol, which were present in the gel and buffer, indicating that amylin forms intermolecular bonds with 4-HNE and MDA. The higher avidity of amylin from humans compared with rodent amylin to bind 4-HNE and MDA is likely due to the larger number of amino acids with binding affinity to reactive aldehydes (K, 2C, and H in human amylin vs. only K and 2C in rat amylin). Additional data showing the anatomical localization of amylin-4HNE adducts are included in Supplementary Fig. 2.

IL-1β Activation in Hearts of Human Amylin–Expressing Diabetic Rats

IL-1β immunoreactivity was detected in HIP rat heart tissue, but not UCD rats (Fig. 5*A*). These results correlate with a

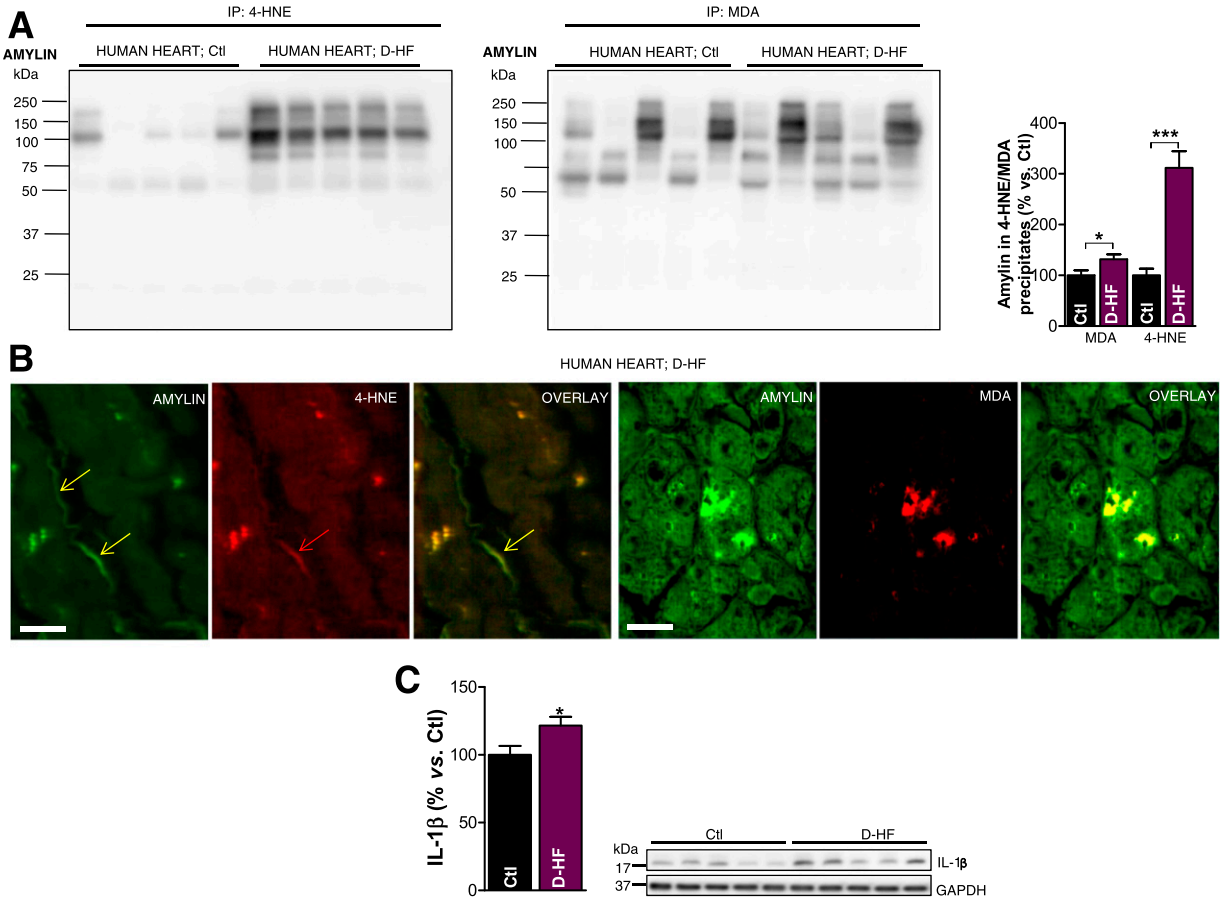

Figure 3—Failing hearts from patients with type 2 diabetes display amylin-4-HNE and amylin-MDA adducts and increased IL-1β synthesis. *A*: Western blot analysis of enriched 4-HNE and MDA fractions immunoprecipitated from the left ventricles of patients with D-HF vs. nondiabetic Ctl subjects. *B*: First three images show dual-immunofluorescence staining of amylin (green) and 4-HNE (red) on transverse sections from left ventricle tissue of patients with D-HF vs. nondiabetic Ctl subjects. Arrows indicate amylin incorporation within the sarcolemma and the subsequent formation of adducts with 4-HNE. The next three images are cross sections of cardiac tissue showing the formation of amylin-MDA adducts within cardiac myocytes. Scale bars, 20 μm. *C*: Western blot analysis of IL-1β in left ventricle tissue of patients with D-HF vs. nondiabetic Ctl subjects. A representative blot from two independent experiments is shown. Data are presented as the mean ± SE. $^{*}P < 0.05$; $^{***}P < 0.001$.

greatly increased IL-1β transcript in HIP rat hearts (Fig. 5*B*), suggesting that cardiac incorporation of aggregated amylin induces expression of IL-1β. Western blot analysis showed increased IL-1β levels in HIP rat hearts (Fig. 5*C*). In contrast, hearts of UCD and WT rats displayed similar IL-1β levels. HIP rats also showed elevated levels of TNF-α, but unchanged levels of IL-6 and IL-10. Compared with WT rats, UCD rats present no significant alteration of cardiac TNF-α, IL-6, and IL-10 cytokine levels (Fig. 5*C*). Thus, the association of aggregated amylin with peroxidative membrane injury and IL-1β synthesis in the hearts of patients in the O-HF group is mirrored in HIP rats, but is absent in UCD rats.

Systemic Effects After Intravenous Injection of Aggregated Amylin in Mice

Aggregated amylin was found in human pancreas, blood, and heart (Fig. 1*B*). Using the Langendorff system and intravenously injected aggregated human amylin in normal mice, we tested the hypothesis that circulating aggregated amylin promotes myocardial amylin accumulation, the generation of reactive aldehydes, and IL-1β synthesis.

Perfusion of isolated hearts with amylin led to amylin deposition on the sarcolemma and in myocardial interstices (Fig. 6*A*, arrows). Western blots further confirmed the incorporation of aggregated amylin in cardiac tissue (Fig. 6*B*) and the formation of amylin-4-HNE and amylin-MDA adducts (Fig. 6*C*). The IL-1β level was similar to that in saline-perfused hearts (Fig. 6*D*). These results demonstrate a direct and rapid effect of circulating aggregated amylin to generate reactive aldehydes in cardiac tissue and suggest that the inflammation response involving IL-1β is downstream of lipid peroxidation.

In contrast to Ctl subjects, mice injected with aggregated human amylin contained amylin-4-HNE and amylin-MDA adducts in cardiac myocyte lysates (Fig. 6*E*). The IL-1β level was also increased in this animal group (Fig. 6*F*). These results confirm that circulating aggregated

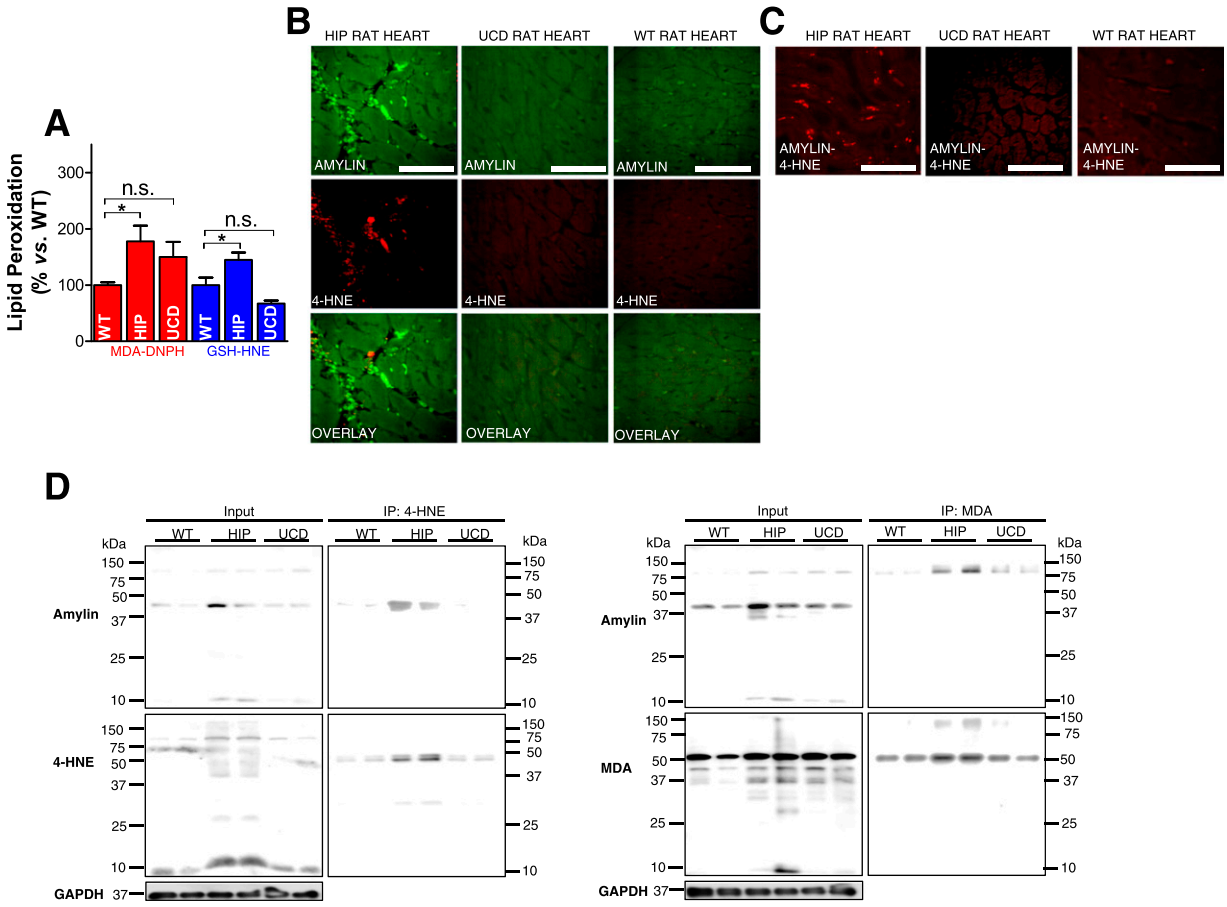

Figure 4—Aggregated amylin induces peroxidative membrane injury in the heart in a HIP rat. *A*: An LC-MS/MS method was applied to measure MDA in rat heart homogenates using derivatization of MDA with DNPH. The same method was applied to measure GSH-HNE in rat heart homogenates. *B*: Dual-immunofluorescence staining of amylin (green) and 4-HNE (red) in heart tissue sections from HIP rats, UCD rats, and WT rats (negative Ctls). *C*: PLA was performed with anti-amylin and anti–4-HNE antibodies on heart sections from WT, HIP, and UCD rats. PLA signal shows an overall consistency with 4-HNE-amylin appearing in clusters. Ten sections per sample from $n = 4$ rats in each group were investigated. Scale bars, 20 μm. *D*: Coimmunoprecipitation (IP)/immunoblot (IB) assays of 4-HNE and MDA (left and right panels, respectively) with amylin from WT, HIP, and UCD rat heart homogenates. Input: IB for amylin, 4-HNE or MDA, and GAPDH in the heart homogenates. IP: Anti–4-HNE and anti-MDA antibodies pulled down more amylin from HIP compared with WT and UCD heart homogenates. A representative blot from two independent experiments is shown. Data are presented as the mean ± SE. *$P < 0.05$, not statistically significant (n.s.).

amylin can induce cardiac peroxidative injury and elevate IL-1β synthesis independently of hyperglycemia.

Mechanism for Amylin-Induced Peroxidative Membrane Injury and IL-1β Expression

To further understand this novel mechanism of sarcolemmal injury, we used an in vitro system where isolated Ctl myocytes were incubated for 2 h with 50 μmol/L human amylin or/and 400 mg/dL glucose. Exposure to 50 μmol/L human amylin for 2 h results in the same level of amylin uptake in myocytes as in HIP rats (7). The lipid peroxide level was measured in single cells using the fluorescent probe C_{11}-BODIPY$^{581/591}$. Compared with WT rats, the lipid peroxide level was increased in myocytes from HIP rats, but not those from UCD rats (Fig. 7*A*). Furthermore, the incubation of Ctl rat myocytes with human amylin (50 μmol/L for 2 h) increased lipid peroxidation (Fig. 7*A*). This result is further supported by Western blot analysis (Fig. 7*B*). In contrast, incubation for the same duration with 400 mg/dL glucose had no effect on the lipid peroxidation level (Fig. 7*A* and *B*). The incorporation of aggregated amylin in cell membranes was then prevented by pretreating isolated Ctl myocytes with 50 μmol/L poloxamer 188 surfactant. Surfactant molecules (S) blocked amylin-induced lipid peroxidation (Fig. 7*C*, magenta bar). In a separate experiment, we quenched basal ROS production in Ctl myocytes by preincubation with NAC, a scavenger of H_2O_2 and HO*. Pretreatment with NAC prevented the ignition of the lipid peroxidation chain reaction, which is induced by incubation with human amylin (Fig. 7*C*, green bar). Thus, impeding the incorporation of aggregated amylin in cellular membranes (e.g., by membrane sealants) or quenching the basal ROS blocked amylin-induced lipid peroxidation in isolated myocytes.

Consistent with our previous data showing that the incubation of isolated cardiac myocytes with aggregated amylin increases ROS production (7), we found significantly

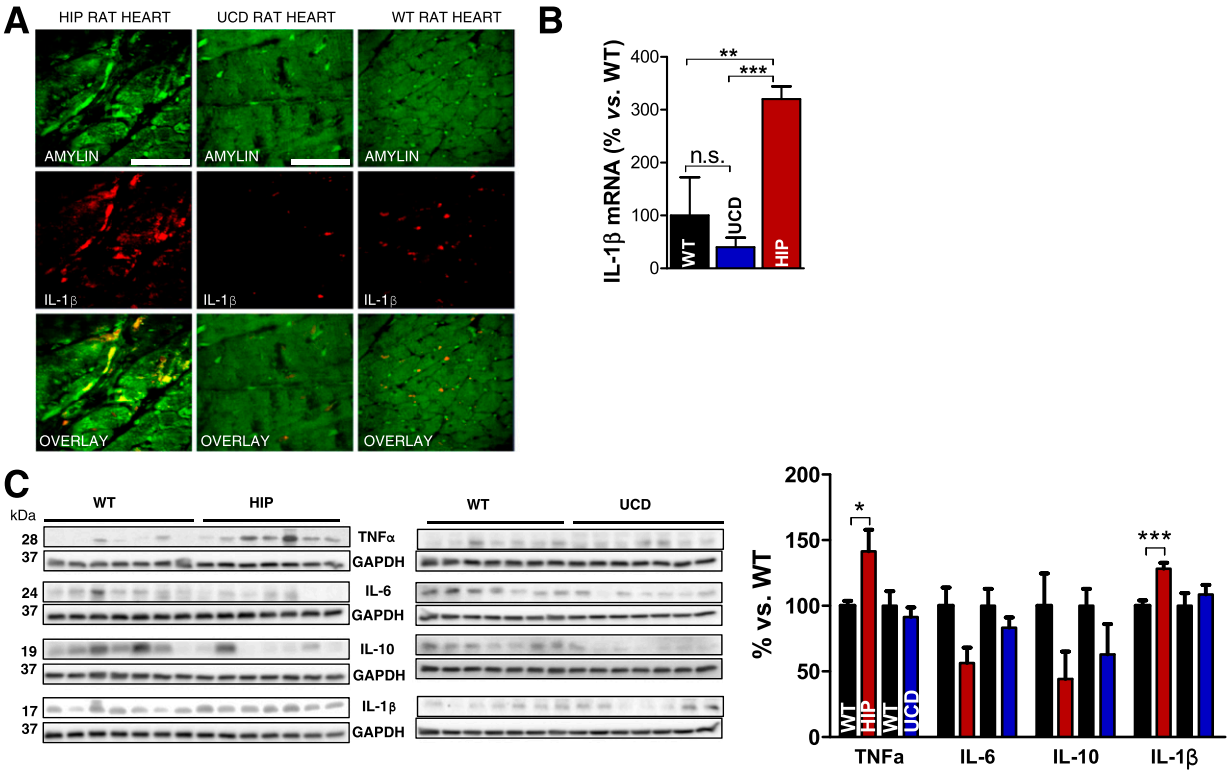

Figure 5—Aggregated amylin increases IL-1β synthesis in the hearts of rats expressing human amylin in the pancreas. *A*: Cardiac tissue from HIP rats was analyzed by immunofluorescence imaging with an IL-1β antibody. Myocyte staining for both amylin (green) and IL-1β (red) are readily observed. Scale bars, 20 μm. In contrast, UCD rats and WT rats (negative Ctls) lacked the IL-1β immunoreactivity signal in cardiac myocytes. Scale bars, 20 μm. *B*: Quantitative RT-PCR data showed elevated IL-1β mRNA levels in heart specimens from HIP rats vs. UCD rats and WT rats. $n = 7$ samples/group. Data are presented as the mean ± SE. *C*: Western blot analysis of IL-1β, TNF-α, IL-6, and IL-10 in hearts from HIP, UCD, and WT rats. A representative blot from two independent experiments is shown. $^{*}P < 0.05$, $^{**}P < 0.01$, $^{***}P < 0.001$, not statistically significant (n.s.).

higher H_2O_2 levels in cardiac myocytes from HIP rats compared with those in UCD rats (Fig. 7*D*). ROSs are considered the proximal signals for the activation of the IL-1β–processing inflammasome in pancreatic islets (3) and heart (33). Intriguingly, recent experimental evidence (34) points to 4-HNE as another activator of signaling cascades underlying IL-1β synthesis and activation. We therefore hypothesized that amylin-mediated peroxidative membrane injury increases IL-1β synthesis. Indeed, the incubation of Ctl myocytes (Fig. 7*E*) with aggregated amylin (50 μmol/L for 2 h) resulted in robust IL-1β synthesis. Preventing amylin-induced lipid peroxidation by impeding amylin incorporation with a membrane stabilizer (Fig. 7*E*, S, magenta bars) or by quenching the basal ROS with NAC (green bars) blocked IL-1β synthesis in cardiac myocytes (Fig. 7*E*). This result is further supported by Western blotting (Fig. 7*F*). In contrast, incubation for the same duration with 400 mg/dL glucose had no effect on IL-1β (Fig. 7*F*).

Based on these data, we propose (Fig. 7*G*) that myocardial amylin deposition destabilizes the sarcolemma and generates reactive aldehydes that perturb intracellular homeostasis, leading to increased synthesis of IL-1β. Blocking either myocyte amylin uptake (by surfactants) (Fig. 7*G*, S) or the lipid peroxidation chain reaction (by NAC) demonstrated that peroxidative membrane injury is upstream of IL-1β–increased synthesis (Fig. 7*G*).

DISCUSSION

The link of diabetes with co-occurring disorders in the heart involves complex multifactorial pathways (17,35) that are still incompletely understood. Prior studies (17,36–40), including our work (36), demonstrated heart dysfunction in rodent models of type 2 diabetes that lack amylin deposition. However, we previously (6,7) showed that HIP rats develop diastolic dysfunction and cardiac hypertrophy even in prediabetes, pointing to amylin deposition as a factor that accelerates the development of diabetic heart disease. From our prior work (6,7) and present results, it appears that the amylin-specific deleterious effects on the heart involve the destabilization of the sarcolemma. We have previously demonstrated that amylin deposition induces sarcolemmal Ca^{2+} leakage, leading to increased levels of myocyte cytosolic Ca^{2+}, the activation of Ca^{2+}-mediated hypertrophy, and the remodeling of signaling pathways (6). Conversely, reducing myocardial amylin deposition improved myocyte Ca^{2+} handling and heart function in HIP rats (7). We now report that hearts

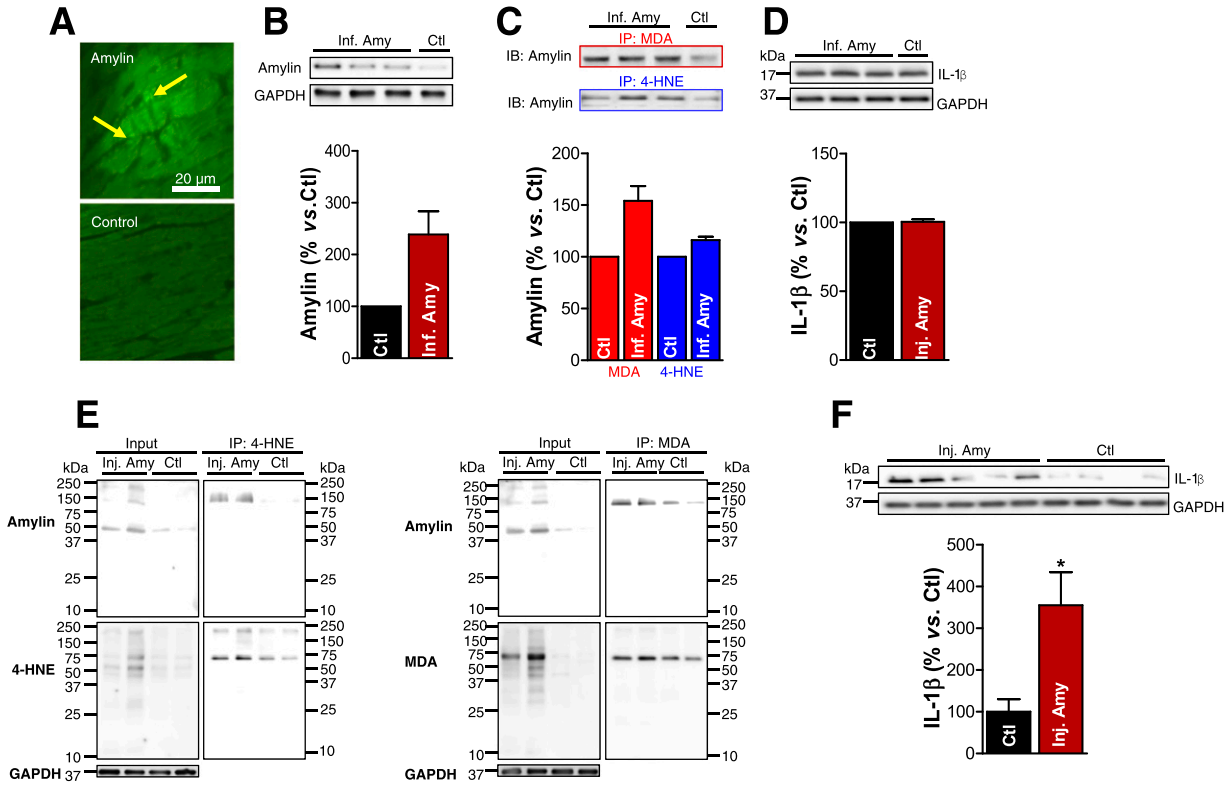

Figure 6—Langendorff perfusion of mice with aggregated amylin leads to the formation of amylin-4-HNE/MDA adducts and IL-1β activation. *A*: The 10 μmol/L biotinylated human amylin was recirculated in an isolated mouse heart on a Langendorff apparatus for 2 h. Fluorescence imaging shows binding of fluorescein isothiocyanate-avidin to the circulated biotinylated human amylin, thus demonstrating amylin deposition (arrows) in the heart. *B–D*: Isolated mouse hearts were perfused with 10 μmol/L aggregated human amylin (n = 3; Inf. Amy) or Tyrode solution (n = 1; Ctl) for 2 h on a Langendorff system, followed by a 10-min washout. *B*: Western blot measurement of amylin incorporated in the Langendorff perfused hearts. *C*: 4-HNE and MDA were immunoprecipitated, and the amylin level in the immunoprecipitate was measured by Western blot. *D*: Western blot analysis of IL-1β in Inf. Amy vs. Ctl hearts. *E*: C57BL/6 mice were intravenously injected with 2 μg/g body wt aggregated human amylin (n = 4; Inj. Amy) or saline (n = 4; Ctl). Coimmunoprecipitation (IP)/immunoblot (IB) assays of 4-HNE and MDA (left and right panels, respectively) with amylin from amylin-injected and Ctl mice heart homogenates. Input: IB for amylin, 4-HNE or MDA, and GAPDH in the heart homogenates. IP: anti–4-HNE and anti-MDA antibodies pulled down more amylin from amylin-injected compared with Ctl mouse heart homogenates. *F*: IL-1β level in hearts from mice injected with human amylin vs. Ctl. A representative blot from two independent experiments is shown. Data are presented as the mean ± SE. *P < 0.05.

accumulating aggregated amylin (i.e., HIP rat hearts) are prone to the generation of reactive aldehydes (4-HNE and MDA) and the formation of amylin-HNE and amylin-MDA adducts. The levels of 4-HNE and MDA in diabetic hearts that lack amylin deposition (i.e., UCD rat hearts) are comparable to those in hearts from WT nondiabetic rats, despite pronounced ROS production (Fig. 7*D*). Furthermore, HIP rat hearts showed hypersynthesis of IL-1β, which is linked to the increased production of reactive aldehydes, as suggested by previous results (34) and our experiments in isolated cells (Fig. 7). This pathologic change is not seen in UCD rat hearts supporting a role of amylin deposition in inducing sarcolemmal injury. Because the generation of reactive aldehydes, the formation of amylin adducts, and the increased IL-1β synthesis in human cardiac tissue appear in association with amylin deposition (Figs. 2 and 3), HIP rats are clinically relevant animal models with which to mechanistically understand this novel pathologic link between type 2 diabetes and heart disease. In Table 1, we summarize alterations to cardiac function/structure associated with amylin deposition in the HIP rat model.

Intriguingly, several bands corresponding to aggregated amylin are seen in cardiac myocytes, but not in blood (Fig. 1*B*), suggesting that amylin may aggregate in situ, within myocytes. This result begs questions regarding the ability of myocytes to degrade intracellular amylin and whether implicated mechanisms are impaired under conditions underlying the amylin incorporation in cardiac myocytes. Therefore, future studies should focus on identifying ways to augment the clearance of cytosolic amylin before its aggregation. Furthermore, the formation of amylin-4-HNE and amylin-MDA adducts suggests the hypothesis that hyperamylinemia increases the production of reactive aldehydes (as demonstrated by data displayed in Figs. 4*A* and 6*E*), which, in turn, may accelerate myocardial amylin deposition via adduct formation. This mechanism is common to Aβ

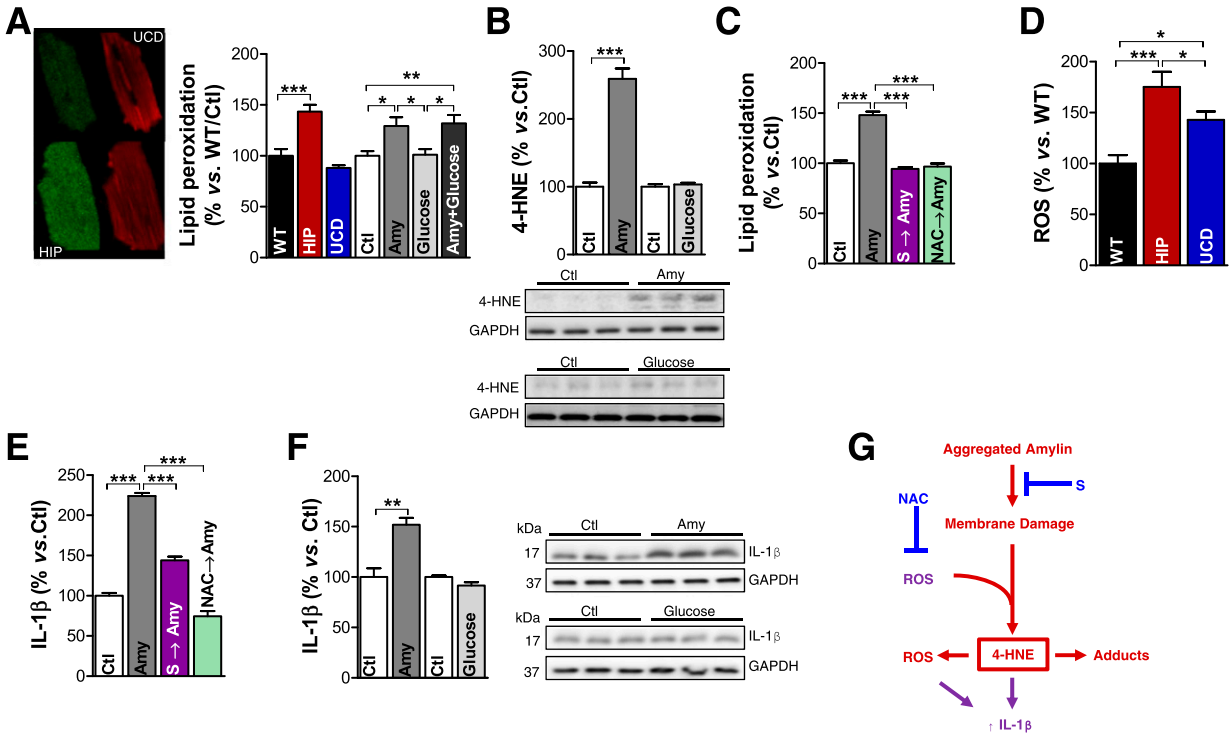

Figure 7—Amylin-mediated peroxidative membrane injury exacerbates ROS production and increases IL-1β synthesis in isolated cardiac myocytes. *A*: Measurement of lipid peroxidation with C_{11}-BODIPY$^{581/591}$ in cardiac myocytes from WT, HIP, and UCD rats, as well as in myocytes incubated with aggregated amylin (Amy) and/or 400 mg/dL glucose. *B*: Western blot analysis of 4-HNE in myocytes incubated with aggregated Amy or 400 mg/dL glucose. *C*: Lipid peroxidation measurements with C_{11}-BODIPY$^{581/591}$ in myocytes incubated for 2 h under Ctl conditions, with aggregated Amy, with 50 μmol/L poloxamer 188 followed by aggregated amylin (S → Amy), and with 5 mmol/L NAC for 30 min followed by aggregated amylin (NAC → Amy). *D*: ROS production, measured with the fluorescent indicator CM-H_2DCFA, was compared in cardiac myocytes from WT, UCD, and HIP rats. *E*: IL-1β level, assessed by immunofluorescence, in isolated Ctl myocytes incubated under the four conditions described in panel *C*. *F*: Western blot analysis of IL-1β in myocytes incubated with aggregated Amy or 400 mg/dL glucose. Ten myocytes/rat; $n = 5$ rats/group. A representative blot from two independent experiments is shown. Data are presented as the mean ± SE. $^*P < 0.05$, $^{**}P < 0.01$, $^{***}P < 0.001$. *G*: Proposed mechanism for amylin-induced lipid peroxidation and IL-1β activation.

pathology in brains of patients with Alzheimer disease (41), but it needs clarification in relation to amylin deposition in the heart. Amylin-induced generation of reactive aldehydes may be of further relevance to various changes in heart metabolism attributed to peroxidative injury (22,38–40). Antioxidants and surfactants inhibited the lipid peroxidation chain reaction and the incorporation of aggregated amylin into cellular membranes, respectively. The use of NAC and a membrane stabilizer was intended to demonstrate a proof of concept and to provide insights into a potential mechanism. Additional studies are needed to assess the mechanisms of action, formulations, and potential side effects.

Table 1—A summary of alterations to cardiac function/structure associated with amylin deposition in the HIP rat model

Cardiac function/structure alteration	Reference
Diastolic dysfunction	6
Eccentric hypertrophy	7
Dilation	7
Arrhythmia	13
Myocyte Ca^{2+} dysregulation	6
Elevated myocyte Na^+	42
Impaired protein biosynthesis	14
Amylin deposition	6,7
ROS production	Present results
Sarcolemmal lipid peroxidation	Present results
Inflammation	Present results

In conclusion, we demonstrated that hyperamylinemia and subsequent elevated blood levels of aggregated amylin promote the incorporation of aggregated amylin within cardiac myocytes, which destabilizes the sarcolemma and generates reactive aldehydes that perturb intracellular homeostasis, leading to increased IL-1β synthesis. Thus, exacerbated synthesis of IL-1β is revealed as a critical stress-activated signaling pathway in response to the interaction of aggregated amylin with myocytes. Given that aggregated amylin triggers IL-1β release in pancreatic islets (3), the present results suggest that pancreatic amylin pathology may be linked with diabetic myocyte injury by amylin deposition in the heart. Future studies need to

determine whether exacerbated IL-1β synthesis in myocytes accumulating aggregated amylin results from the activation of the NLRP3 inflammasome, which thus might function as a sensor of myocyte amylin uptake and a potential mediator of myocyte injury.

Funding. This research was supported by the National Institutes of Health/National Heart, Lung, and Blood Institute (grants R01-HL-105993 to K.B.M., R01-HL-109501 to S.D., and R01-HL-118474 to F.D.) and the National Science Foundation Division of Chemical, Bioengineering, Environmental, and Transport Systems (grant CBET 1357600 to F.D.). HPLC analysis was performed in a National Institute of General Medical Sciences–supported protein core (National Heart, Lung, and Blood Institute grant 5P20GM103486 to L.B.H.), while proteomics analysis was performed in the University of Kentucky Proteomics core. The LC-MS/MS equipment was acquired using a National Center for Research Resources High-End Instrumentation grant (S10 RR029127 to H.Z.).

Duality of Interest. No potential conflicts of interest relevant to this article were reported.

Author Contributions. M.L. performed experiments that included immunoblotting, HPLC, LC-MS/MS, lipid peroxidation for myocytes, and animal injection and helped with the editing of the manuscript. N.V. performed all double-immunofluorescence staining, confocal imaging, and RT-PCR experiments, including data analysis. X.P. and S.S. performed animal surgeries and metabolic characterization of the animals. A.M. conducted the LC-MS/MS analysis for assessing lipid peroxidation in animal models. M.C. and L.B.H. performed and analyzed the HPLC experiments. J.C. and H.Z. performed and analyzed the proteomic experiments. M.G.N. contributed to the design of the inflammation study. K.B.M. isolated and prepared the human cardiac tissue and contributed to the design of the study. S.D. performed the reactive oxygen species experiments in isolated cardiac myocytes and contributed to the design of the study. F.D. conceived the project and wrote the manuscript with assistance from the other authors. F.D. is the guarantor of this work and, as such, had full access to all the data in the study and takes responsibility for the integrity of the data and the accuracy of the data analysis.

References

1. Westermark P, Andersson A, Westermark GT. Islet amyloid polypeptide, islet amyloid, and diabetes mellitus. Physiol Rev 2011;91:795–826
2. Zraika S, Hull RL, Udayasankar J, et al. Oxidative stress is induced by islet amyloid formation and time-dependently mediates amyloid-induced beta cell apoptosis. Diabetologia 2009;52:626–635
3. Masters SL, Dunne A, Subramanian SL, et al. Activation of the NLRP3 inflammasome by islet amyloid polypeptide provides a mechanism for enhanced IL-1β in type 2 diabetes. Nat Immunol 2010;11:897–904
4. Netea MG, van de Veerdonk FL, van der Meer JW, Dinarello CA, Joosten LA. Inflammasome-independent regulation of IL-1-family cytokines. Annu Rev Immunol 2015;33:49–77
5. Gong W, Liu ZH, Zeng CH, et al. Amylin deposition in the kidney of patients with diabetic nephropathy. Kidney Int 2007;72:213–218
6. Despa S, Margulies KB, Chen L, et al. Hyperamylinemia contributes to cardiac dysfunction in obesity and diabetes: a study in humans and rats. Circ Res 2012;110:598–608
7. Despa S, Sharma S, Harris TR, et al. Cardioprotection by controlling hyperamylinemia in a "humanized" diabetic rat model. J Am Heart Assoc 2014;3:e001015
8. Jackson K, Barisone GA, Diaz E, Jin LW, DeCarli C, Despa F. Amylin deposition in the brain: a second amyloid in Alzheimer disease? Ann Neurol 2013;74:517–526
9. Fawver JN, Ghiwot Y, Koola C, et al. Islet amyloid polypeptide (IAPP): a second amyloid in Alzheimer's disease. Curr Alzheimer Res 2014;11:928–940
10. Oskarsson ME, Paulsson JF, Schultz SW, Ingelsson M, Westermark P, Westermark GT. In vivo seeding and cross-seeding of localized amyloidosis: a molecular link between type 2 diabetes and Alzheimer disease. Am J Pathol 2015;185:834–846
11. Srodulski S, Sharma S, Bachstetter AB, et al. Neuroinflammation and neurologic deficits in diabetes linked to brain accumulation of amylin. Mol Neurodegener 2014;9:30
12. Srodulski S, Loria A, Despa S, Despa F. Abstract 13963: hyperamylinemia, a potential therapeutic target in diabetic cardiorenal syndrome. Circulation 2014;130:A13963
13. Erickson JR, Pereira L, Wang L, et al. Diabetic hyperglycaemia activates CaMKII and arrhythmias by O-linked glycosylation. Nature 2013;502:372–376
14. Ilaiwy A, Liu M, Parry TL, et al. Human amylin proteotoxicity impairs protein biosynthesis, and alters major cellular signaling pathways in the heart, brain and liver of humanized diabetic rat model in vivo. FASEB J 2016;30(Suppl.):lb461
15. Verma N, Ly H, Liu M, et al. Intraneuronal amylin deposition, peroxidative membrane injury and increased IL-1β synthesis in brains of Alzheimer's disease patients with type-2 diabetes and diabetic HIP rats. J Alzheimers Dis 2016;53:259–272
16. Matveyenko AV, Butler PC. Islet amyloid polypeptide (IAPP) transgenic rodents as models for type 2 diabetes. ILAR J 2006;47:225–233
17. Bugger H, Abel ED. Molecular mechanisms of diabetic cardiomyopathy. Diabetologia 2014;57:660–671
18. Querfurth HW, Suhara T, Rosen KM, et al. Beta-amyloid peptide expression is sufficient for myotube death: implications for human inclusion body myopathy. Mol Cell Neurosci 2001;17:793–810
19. Janson J, Ashley RH, Harrison D, McIntyre S, Butler PC. The mechanism of islet amyloid polypeptide toxicity is membrane disruption by intermediate-sized toxic amyloid particles. Diabetes 1999;48:491–498
20. Engel MF, Khemtémourian L, Kleijer CC, et al. Membrane damage by human islet amyloid polypeptide through fibril growth at the membrane. Proc Natl Acad Sci U S A 2008;105:6033–6038
21. Huang CJ, Haataja L, Gurlo T, et al. Induction of endoplasmic reticulum stress-induced beta-cell apoptosis and accumulation of polyubiquitinated proteins by human islet amyloid polypeptide. Am J Physiol Endocrinol Metab 2007;293:E1656–E1662
22. Srivastava SK, Ramana KV, Bhatnagar A. Role of aldose reductase and oxidative damage in diabetes and the consequent potential for therapeutic options. Endocr Rev 2005;26:380–392
23. Cummings BP, Digitale EK, Stanhope KL, et al. Development and characterization of a novel rat model of type 2 diabetes mellitus: the UC Davis type 2 diabetes mellitus UCD-T2DM rat. Am J Physiol Regul Integr Comp Physiol 2008;295:R1782–R1793
24. Griffen SC, Wang J, German MS. A genetic defect in beta-cell gene expression segregates independently from the fa locus in the ZDF rat. Diabetes 2001;50:63–68
25. Yang L, Gal J, Chen J, Zhu H. Self-assembled FUS binds active chromatin and regulates gene transcription. Proc Natl Acad Sci U S A 2014;111:17809–17814
26. Czauderna M, Kowalczyk J, Marounek M. The simple and sensitive measurement of malondialdehyde in selected specimens of biological origin and some feed by reversed phase high performance liquid chromatography. J Chromatogr B Analyt Technol Biomed Life Sci 2011;879:2251–2258
27. Despa S, Bers DM. Functional analysis of Na+/K+-ATPase isoform distribution in rat ventricular myocytes. Am J Physiol Cell Physiol 2007;293:C321–C327
28. Collins JM, Despa F, Lee RC. Structural and functional recovery of electropermeabilized skeletal muscle in-vivo after treatment with surfactant poloxamer 188. Biochim Biophys Acta 2007;1768:1238–1246
29. Kahn SE, D'Alessio DA, Schwartz MW, et al. Evidence of cosecretion of islet amyloid polypeptide and insulin by beta-cells. Diabetes 1990;39:634–638
30. Kruger DF, Gatcomb PM, Owen SK. Clinical implications of amylin and amylin deficiency. Diabetes Educ 1999;25:389–397; quiz 398

31. Enoki S, Mitsukawa T, Takemura J, et al. Plasma islet amyloid polypeptide levels in obesity, impaired glucose tolerance and non-insulin-dependent diabetes mellitus. Diabetes Res Clin Pract 1992;15:97–102
32. Johnson KH, O'Brien TD, Jordan K, Westermark P. Impaired glucose tolerance is associated with increased islet amyloid polypeptide (IAPP) immunoreactivity in pancreatic beta cells. Am J Pathol 1989;135:245–250
33. Ghigo A, Franco I, Morello F, Hirsch E. Myocyte signalling in leucocyte recruitment to the heart. Cardiovasc Res 2014;102:270–280
34. Herndon AM, Breshears MA, McFarlane D. Oxidative modification, inflammation and amyloid in the normal and diabetic cat pancreas. J Comp Pathol 2014;151:352–362
35. Ingelsson E, Sundström J, Arnlöv J, Zethelius B, Lind L. Insulin resistance and risk of congestive heart failure. JAMA 2005;294:334–341
36. Guglielmino K, Jackson K, Harris TR, et al. Pharmacological inhibition of soluble epoxide hydrolase preserves cardiac myocyte structure and function in hyperglycemic rats. Am J Physiol Heart Circ Physiol 2012;303:H853–H862
37. Bugger H, Abel ED. Rodent models of diabetic cardiomyopathy. Dis Model Mech 2009;2:454–466
38. Benderdour M, Charron G, DeBlois D, Comte B, Des Rosiers C. Cardiac mitochondrial NADP+-isocitrate dehydrogenase is inactivated through 4-hydroxynonenal adduct formation: an event that precedes hypertrophy development. J Biol Chem 2003;278:45154–45159
39. Choksi KB, Boylston WH, Rabek JP, Widger WR, Papaconstantinou J. Oxidatively damaged proteins of heart mitochondrial electron transport complexes. Biochim Biophys Acta 2004;1688:95–101
40. Lashin OM, Szweda PA, Szweda LI, Romani AM. Decreased complex II respiration and HNE-modified SDH subunit in diabetic heart. Free Radic Biol Med 2006;40:886–896
41. Arimon M, Takeda S, Post KL, Svirsky S, Hyman BT, Berezovska O. Oxidative stress and lipid peroxidation are upstream of amyloid pathology. Neurobiol Dis 2015;84:109–119
42. Lambert R, Srodulski S, Peng X, Margulies KB, Despa F, Despa S. Intracellular Na+ concentration ([Na+]i) is elevated in diabetic hearts due to enhanced Na+-glucose cotransport. J Am Heart Assoc 2015;4: e002183